Available online at www.sciencedirect.com
ScienceDirect
Acta Materialia 58 (2010) 6609–6618
Acta MATERIALIA
www.elsevier.com/locate/actamat

Hydride precipitation and stresses in zircaloy-4 observed by synchrotron X-ray diffraction

J.R. Santisteban [a,*], M.A. Vicente-Alvarez [a], P. Vizcaíno [b], A.D. Banchik [b], J.D. Almer [c]

[a] CONICET and Instituto Balseiro, Centro Atómico Bariloche, Argentina
[b] Centro Atómico Ezeiza, CNEA, Buenos Aires, Argentina
[c] Advanced Photon Source, Argonne National Laboratory, Argonne, IL, USA

Received 13 April 2010; received in revised form 18 August 2010; accepted 18 August 2010
Available online 16 September 2010

Abstract

The grain stresses within hydrides precipitated in rolled zircaloy-4 plates were determined by synchrotron X-ray diffraction experiments using an 80 keV photon beam and a high-speed area detector placed in transmission geometry. Results showed large compressive stresses (360 ± 20 MPa) in the hydrides along the plate rolling direction. The origin of these stresses was investigated by performing hydride dissolution/precipitation in situ for thermal cycles between room temperature and 400 °C. A large stress hysteresis was observed, with a steady decrease on heating and an abrupt change on cooling. The observed stresses are explained by the constraint imposed by grain boundaries on the growth of hydride platelets on the rolling–transverse plane of the rolled plates.

Keywords: Internal stresses; Hydrides; Precipitation; Texture; Zirconium

1. Introduction

Zirconium hydride precipitates in zirconium alloys with a characteristic acicular or plate morphology which can be easily observed by optical microscopy. These hydrides usually lead to marked embrittlement of the material, especially when they are oriented along the radial direction of tubes. Hydride precipitation in Zr alloys is a complex process, and the effect that factors such as grain size, texture and applied or residual stresses have on the final morphology of the hydrides has been extensively reported in the literature. For instance, upon the application of a stress, hydrides tend to precipitate perpendicular to a tensile axis or parallel to a compression axis [1,2]. So, repeated thermal cycling under stress can steadily increase the proportion of detrimental hydrides either in service or under dry storage conditions [3]. Residual stresses also influence hydride precipitation, so compressive radial strains are introduced by cold working in the last manufacturing stages of tubing, in order to avoid the formation of radial hydrides.

Transmission electron microscopy (TEM) observations revealed that, on a microscopic scale, the "macroscopic" hydrides seen under the optical microscope are composed of stacks of hydride plates sharing a common habit plane [4]. The individual plates in a stack grow by a displacive transformation, which involves both shear and local volume change in the parent lattice. Perovic et al. [5] proposed that these stacks are formed by repeated nucleation and growth of plates, which eventually coalesce and grow into macroscopic hydride platelets. In this "auto-catalytic" nucleation mechanism, the stress field of a larger parent hydride plate would help to nucleate a smaller daughter hydride, resulting in the offset stacks observed experimentally. So, the orientation of the hydrides stack is determined by the interaction between the strain fields of neighbouring hydride plates. A clear distinction is made between hydrides precipitated at grain boundaries (inter-granular hydrides) from those precipitated across a grain (intra-granular hydrides), as the stress field and the availability of heterogeneous nucleation sites are very different between these two cases.

* Corresponding author. Tel./fax: +54 2944 445154.
E-mail address: J.R.Santisteban@cab.cnea.gov.ar (J.R. Santisteban).

1359-6454/$36.00 © 2010 Acta Materialia Inc. Published by Elsevier Ltd. All rights reserved.
doi:10.1016/j.actamat.2010.08.022

Despite the basic and technological importance that both residual and applied stresses play on zirconium hydrides, there is still a lack of experimental information concerning the magnitude and the nature of the stresses existing *within* the hydrides. The high X-ray flux available in modern synchrotron facilities has recently opened the possibility of studying the minority hydride phase in great detail, so several findings about the hydride response under externally applied stresses have been reported over the last year. Two works [6,7] reported the evolution of hydride strains during uniaxial loading of zircaloy containing between 100 and 400 wt. ppm of hydrogen. Steuwer et al. [6] interpreted the large peak shifts observed for the hydrides as a stress-induced transformation between the δ and γ phases of the hydride, while Kerr et al. [7] concentrated on identifying the mechanical response and mechanisms of load transfer from the Zr matrix to the minority hydride phase. Other works [8–10] studied hydride stresses and precipitation near notches in CT specimens. Kerr et al. reported that, for 60 wt. ppm hydrides precipitated in Zr–2.5Nb, the strain field within the hydride is controlled by the stress state of the matrix [8], and hydride precipitation relaxes the strain field at the crack tip [9]. All these recent works have exploited the shifts observed in the hydride diffraction peaks measured along one or two directions of the sample, in order to determine the relative strain difference from an unknown initial state. The present work reports synchrotron X-ray diffraction experiments aiming to characterize and understand such an initial state, i.e., the large residual stresses usually existing within the hydrides precipitated in unstressed specimens, and hence obtain an insight into the physical mechanisms involved during zirconium hydride precipitation.

2. Samples

The material used in this work is warm-rolled zircaloy-4 plates 6 mm thick, produced by Wah Chang, USA (ASTM B352, Grade R60804). The test specimens are 60 mm along the plate rolling direction (RD), 2.8 mm along the plate normal direction (ND), and 1.8 mm along the plate transverse direction (TD). In order to investigate the effect of zircaloy microstructure on hydride stresses, specimens from two locations of the heat-affected zone (HAZ) of a butt weld joining two plates were also machined. The geometry of the specimens relative to the weld is displayed in Fig. 1a. The two plates were welded along the RD by plasma arc welding, reproducing the geometry of welds used for the manufacture of the reflector vessel for OPAL, a research reactor at ANSTO, Australia. Specimens Z1 and Z2 (not shown in the figure) were taken from the HAZ at 0.5 mm and 5 mm from the fusion zone (FZ), respectively, and specimen Z3 was produced from the original plate. Any macroscopic stresses left by the welding process are expected to be relaxed owing to the small dimensions of the specimens.

Hydride contents of ~200 wt. ppm were introduced in two stages. Initially, a hydride surface layer was deposited by the cathodic charge technique, followed by annealing under a N_2 atmosphere for 24 h at 400 °C, to diffuse the hydrogen into the bulk. The samples were carefully polished to remove the oxide and any remaining hydride layer. The actual concentrations achieved for each specimen were defined from X-ray experiments described later. Fig. 1b and c shows the microstructure of specimens Z3 and Z1 along the ND–RD direction, as observed in the microscope under polarized light, after polishing and etching of the

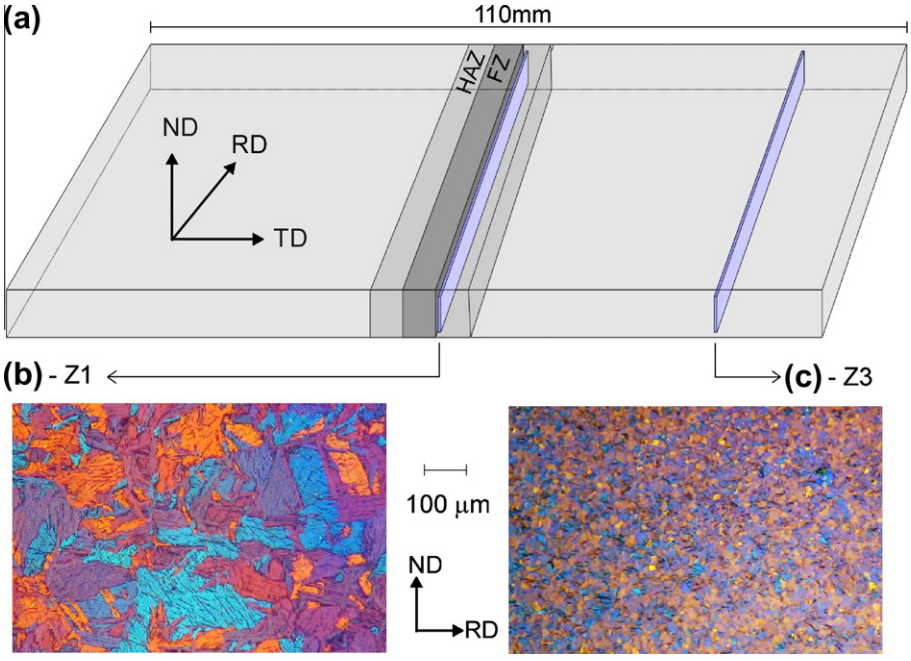

Fig. 1. (a) Geometry of the zircaloy-4 weld, showing the geometry and location of the specimens studied in this work. (b) Polarized-light micrograph of the Z1 specimen, taken form the HAZ of the weld, very close to the FZ. (c) Micrograph of the Z3 specimen, taken from the original rolled plate.

samples following the procedures described in Ref. [11]. Different colours correspond to different grain orientations, and hydrides appear as dark-blue lines. The original zircaloy-4 plate (Z3) has the typical equiaxed grain structure of annealed rolled plates, with diameters from 10 to 20 μm. A thorough characterization of this material has been presented in Ref. [12]. A detail of the Z3 microstructure is shown in Fig. 2. Both intra-granular and inter-granular hydrides are observed, which are preferentially aligned along the RD of the plate. The hydrides appear as lines going from side to side of a grain, indicating that the hydrides correspond to a full cross section of a grain on the RD–TD plane of the plate. All hydrides are restricted to individual grains, with no hydrides traversing across grain boundaries. Hydrides precipitated in the Z1 specimen are different, as drastic changes in microstructure occur across the HAZ of the weld. The temperature reached during welding is high enough to cause a phase change from the hexagonal α-phase into the cubic (bcc) β-phase, followed by a return to the α-phase on cooling. These two phase changes alter the grains shape and size and the crystallographic texture from that of the original base plate. So, the microstructure of the HAZ consists of coarse, plate-like structures with irregular and jagged boundaries called "lenticular α" in Ref. [13]. These coarse structures increase in size as the HAZ approaches the weld pool, reaching sizes up to ~200 μm in the Z1 specimen shown in Fig. 1b. Mostly intra-granular hydrides are observed in the Z1 specimen, which appear as dashed parallel lines of up to ~80 μm length within the large Zr grains. Two "macroscopic" hydride orientations are usually observed within each grain.

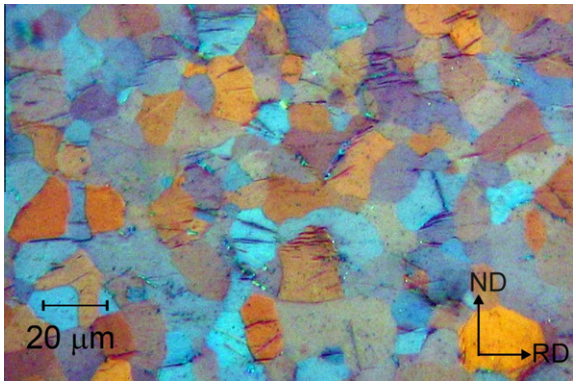

Fig. 2. Detail of the microstructure of the Z3 specimen, taken from the original rolled plate. The hydrides appear as dark-blue lines going from side to side of the grains (For interpretation of the references to colour in this figure legend, the reader is referred to the web version of this article.).

3. Experimental

X-ray diffraction experiments on the specimens were performed at beamline 1-ID of the Advanced Photon Source at Argonne National Laboratory [14], using the experimental arrangement shown in Fig. 3. The beamline was used in Debye–Scherrer transmission geometry, with a monochromatic beam of 0.15 Å wavelength (80 keV) and a size of 300 × 300 μm^2; in conjunction with a high-speed area detector composed of 2048 × 2048 with 200 × 200 μm^2 pixel size, located 2 m from the sample. This geometry allows a number of full diffraction rings to be recorded within a very short time (~1 s), providing information which is averaged over the full thickness of the sample, while thermal or mechanical tests are performed in situ on the specimen. The specimen was aligned with the TD of the original plate parallel to the incident X-ray beam. Owing to the small diffraction angles involved, the detector is essentially exploring all the

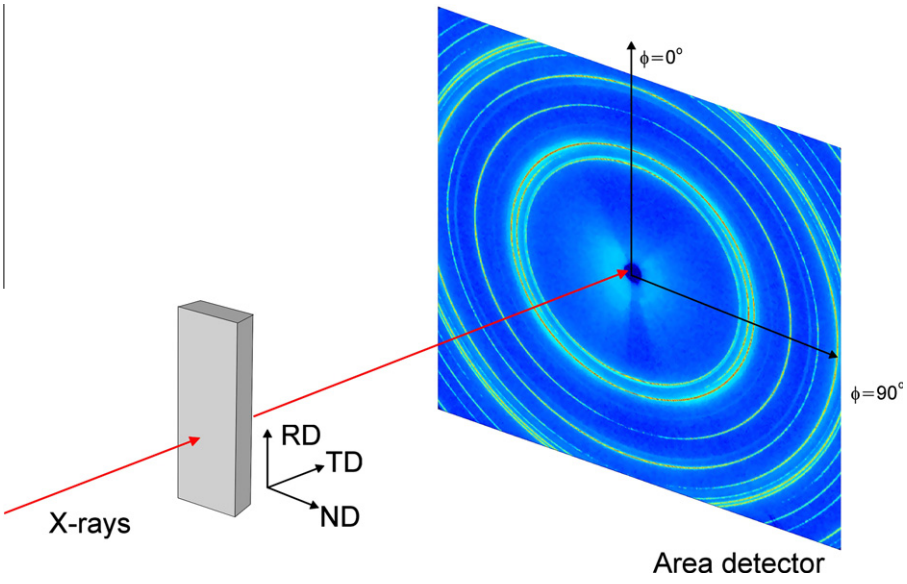

Fig. 3. Schematic representation of the experimental arrangement, indicating the orientation of the specimen, the incident X-ray beam and the area detector. Directions RD, TD and ND are relative to the geometry of the original rolled plate, shown in Fig. 1.

directions in the RD–ND plane of the original plate. For the hydride concentrations introduced in the specimens (~200 wt. ppm), the hydrides dissolve in zircaloy-4 at ~380 °C [15], so the samples were thermally cycled between room temperature and 400 °C in order to study the evolution of crystallographic texture and inter-granular stresses of the hydride phase during the dissolution and precipitation of the hydrides. The specimens were surrounded by an optical furnace which did not interfere with the X-ray beam. The samples were in contact with air; no special atmosphere was applied. The temperature was measured with a type-K thermocouple spot-welded to the sample, which also provided the feedback for the temperature control. For all the thermal cycles, a heating rate of 1 °C s^{-1} was used, and the cooling was done by turning the furnace off, which resulted in an initial cooling rate of ~1 °C s^{-1}. Diffraction patterns were acquired continuously, at a rate of one every 1.1 s. Ten images were added together prior to the data analysis, in order to improve the statistical quality of the data. The basic data analysis procedure consists of correcting the image by dark current, flat-field and spatial distortion corrections [14], in order to obtain intensities that depend only on the sample and the diffraction geometry. After defining a centre, the corrected image is transformed into a series of 2θ diffractograms which are analysed as conventional θ–2θ scans. The Debye rings were divided into 72 azimuths, so each diffractogram corresponds to an angular section or "piece of cake" with a width of 5°. Typical diffraction images for the three specimens are displayed in Fig. 4a. The colour scheme is proportional to the logarithm of the number of counts. The images reflect the microstructural differences between specimens. The Z3 sample displays smooth Debye rings characteristic of hot-rolled Zr, while spotty rings are clearly visible in the Z1 specimen. Two typical diffractograms are shown in the bottom figure, in this case corresponding to the $\phi = 45°$ azimuth of the Z3 specimen at room temperature and at 400 °C. The α-Zr diffractogram is clearly textured, dominated by a strong α(1 0 −1 1) reflection. The presence of hydride precipitates is revealed by small peaks from the δ phase of zirconium hydride. This phase possesses a face centred cubic (fcc) structure and is clearly manifest at room temperature through the δ(1 1 1), δ(2 0 0) and δ(2 2 0) diffraction peaks. No other hydride phases could be observed for any of the specimens studied. A very small intensity is still seen under the δ(1 1 1) peak at 400 °C, indicating that the hydrides are not completely dissolved at this temperature. Some very small hydride peaks were also visible for the Z1 specimen at 400 °C, while for the Z2 specimen all hydride peaks have completely disappeared at this temperature. A small peak observed at 2.15 Å is presumably due to a second phase precipitate but it has not been indexed here.

For all diffractograms, the position, integrated intensity and width of all the accessible peaks from these two phases were determined by least-squares refinement using a Pseudo-Voigt profile. This corresponds to the (1 1 1), (2 0 0) and (2 2 0) of the hydride phase, and (1 0 −1 0), (0 0 0 2), (1 1 −2 0), (1 0 −1 1), (1 0 −1 2), (1 0 −1 3) and (1 1 −2 2) of the α-Zr phase. Most peaks were well isolated

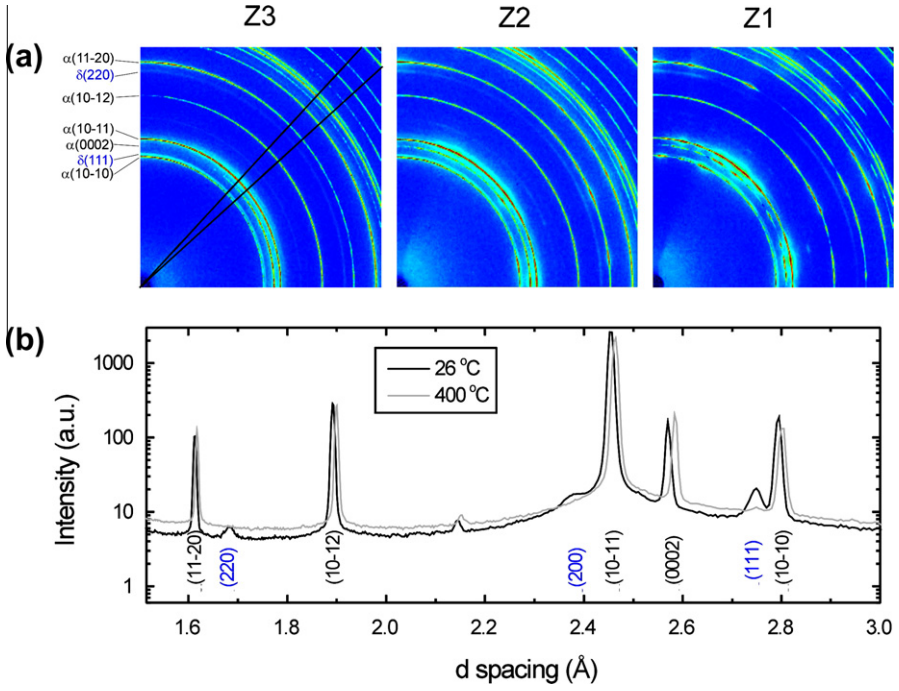

Fig. 4. (a) Typical images recorded by the area detector for the three specimens studied in this work. For better clarity, the colour scheme is proportional to logarithm of the counts, and only a quarter of the image is shown. Debye rings corresponding to the α-Zr and δ-hydride have been indexed. (b) Diffractograms at room temperature and at 400 °C for the specimen taken from the original plate, obtained from the $42.5 < \phi < 47.5°$ azimuth section indicated in the Z3 image.

and could be individually refined. The exceptions were the doublets {δ(1 1 1)–α(1 0 −1 0)}, {δ(2 0 0)–α(1 0 −1 1)} and {α(1 1 −2 2)–α(2 0 −2 1)} which needed to be refined together. Average values of lattice parameters and peak widths for the three samples are presented in Table 1, which is discussed in the following section. The hydrogen contents for each sample are also included in the table, as given by comparing the peak intensities from the two phases using the weighting factors described in Ref. [16]. As only δ hydrides were present in the samples, it was not necessary to take into account γ or ε hydrides to calculate the total hydrogen content. Results from comparison of two pairs of peaks, {δ(1 1 1)–α(1 0 −1 0)} and {δ(2 2 0)–α(1 1 −2 0)}, are listed in order to provide an idea of the uncertainty of the method. The hydrogen contents are ∼180 wt. ppm, near the values expected from the H charging procedure.

A single diffraction image recorded by the area detector provides a wealth of information about the volume fraction, the texture and the stress state of the crystallographic phases present in the samples. The systematic intensity variations around the rings seen in the diffraction image contain texture information which can be used to capture the orientation distribution functions (ODF) for both the Zr grains and the hydrides. In particular, Ref. [17] showed that it is possible to determine the ODF of α-Zr from the information contained in a single diffraction image. Finally, the extremely small distortion of a Debye ring from a perfect circle allows the determination of the strain field that exists in each of the two phases on the RD–ND plane of the specimen [14]. The methods used to perform such analyses from a single diffraction image have been described extensively elsewhere. Specific details used for the present study are provided in the next section.

4. Results

4.1. Texture analysis

The peak areas obtained for the 72 azimuth angles of all diffraction rings belonging to the same phase constitute a set of multiple incomplete pole figures. This information was used to determine the ODF of both the hydrides and the Zr crystallites in the three samples, essentially following the procedure described in Ref. [17]. The main difference from that work is that the MTEX algorithm [18] was used to determine the ODF from the incomplete pole figures in the present study, rather than the E-WIMV algorithm used there. No sample symmetry was imposed to compute the ODF. Details about the determination of the ODF of zirconium hydride are presented elsewhere [19]. On the left of Fig. 5, the pole figures of the δ-hydride phase are shown for the three specimens at room temperature, recalculated from the experimental ODF. The incomplete experimental pole figures used as input for the MTEX algorithm correspond to the central vertical line of the figures (the RD–ND plane). This is the first determination of zirconium hydride pole figures using synchrotron X-ray diffraction. The figures reveal the differences existing between hydrides precipitated at the parent metal and at the HAZ of the weld. The texture indexes are very low in all cases, $t_{Z3} = 1.22$ in the parent plate; and $t_{Z1} = 1.34$ and $t_{Z2} = 1.14$ in the HAZ of the weld.

The pole figures can be explained by considering the orientation relationship observed between the cubic δ-hydride phase and the hexagonal α-Zr where it grows. For recrystallized zircaloy 2 loaded with 250 wt. ppm H, Ref. [20] reports that the most common relations are δ(1 1 1)// α(0 0 0 1) and δ[0 1 1]//α[1 1 −2 0], i.e., a direct correspondence between the close packed planes and directions of both phases, in agreement with earlier work. The texture of the δ hydrides can be predicted by applying the two orientation relationships to the ODF of the α-Zr phase. The ODF for the α-Zr phase, not shown here, were also obtained from the present analysis and confirmed results obtained previously by neutron diffraction experiments [12]. The texture of the original rolled plate (Z3) can be idealized as being composed of two Zr grains with their *c*-axes lying on the ND–TD plane at angles of ±33° to the ND. For the HAZ, the ODF of the Z1 and Z2 specimens present several texture components which result from the $\alpha \rightarrow \beta \rightarrow \alpha$ phase transformation occurring during welding. The main additional texture component corresponds to Zr grains with their *c*-axis lying on the ND–RD plane,

Table 1
Lattice parameters of the hydride unit cell for the three specimens studied in this work. The *a* value reports the ring average, while a_{ND} and a_{RD} reports values measured along the ND and RD of the plates. Results obtained from the δ(1 1 1) and δ(2 2 0) Debye rings are included. Typical uncertainty is in the last significant digit. The difference Δ*a* in the lattice parameter measured along RD and ND is expressed as strain (1 με = 10^{-6}). The relative FWHM along the two directions have been corrected by instrumental resolution. The reported hydrogen content results from analysis of the intensity of the corresponding diffraction peak.

	δ(1 1 1)			δ(2 2 0)		
	Z1	Z2	Z3	Z1	Z2	Z3
a (Å)	4.7588	4.7563	4.7524	4.7576	4.7573	4.7566
a_{ND} (Å)	4.7602	4.7528	4.7423	4.7560	4.7498	4.7437
a_{RD} (Å)	4.7564	4.7608	4.7651	4.7539	4.7607	4.7627
Δ*a* (με)	-800	1700	4800	-430	2300	4000
FWHM ND (με)	5600	4800	5700	9400	8400	8800
FWHM RD (με)	4500	5200	6300	9800	8400	9700
H content (wt. ppm)	235	146	180	206	111	176

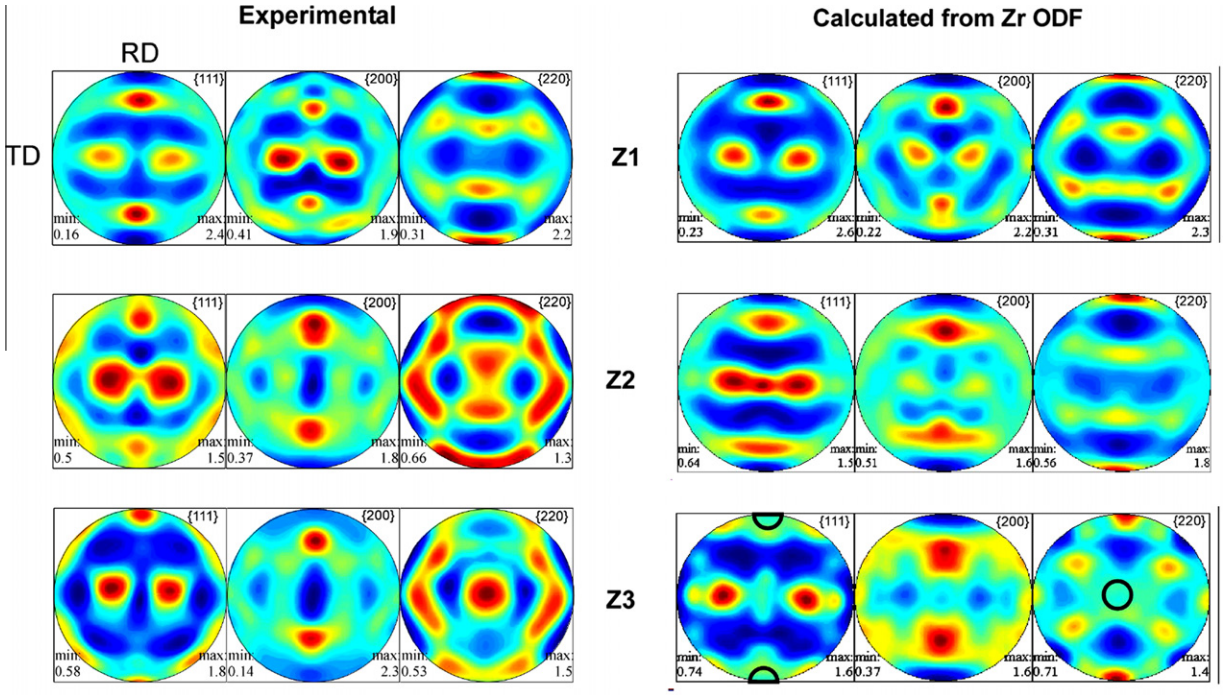

Fig. 5. Pole figures for the zirconium hydride precipitated in the HAZ of the weld (Z1 and Z2), and in the original plate (Z3). Left: experimental results obtained from an analysis of a single diffraction image. Right: Calculated pole figures, from experimental pole figure of α-Zr and the δ(1 1 1)//α(0 0 0 1) and δ[0 1 1]//α[1 1 −2 0] orientation relationship.

a typical feature of welded zirconium-alloy plates with important technological implications, as this makes the HAZ more susceptible to delayed hydride cracking [21].

The pole figures calculated by applying the δ–α orientation relationships to the Zr ODF are displayed on the right of Fig. 5. The calculations agree very well with the experimental pole figure for the Z1 specimen, and predict most of the features observed in the Z2 and Z3 specimens. The results indicate that, for Z1, most of the hydrides transform in accord with such relationships. Larger discrepancies between experimental and predicted pole figures are observed for the hydrides in the original plate (Z3). As indicated by black circles in the calculated pole figure, a texture component with poles with δ(2 2 0)//ND and δ(1 1 1)//RD is seen in the experiment, but not predicted by the calculation. The 90° angle between the two poles suggests that it comes from defined α-Zr orientations. This extra component can be ascribed to the transformation of Zr grains with their α(0 0 0 2)//RD and α(1 1 −2 0)//ND. It was confirmed that Zr grains with such orientation are indeed present in the specimen. At this stage, it is not possible to define the reason for grains of this orientation being more prone to hydride precipitation than the rest. However, these results suggest that a separate stress analysis should be performed on these grains.

4.2. Strains and stresses at room temperature

The variation in the interplanar distance d_{hkl} around the δ(1 1 1) and δ(2 2 0) Debye rings at room temperature is displayed in Fig. 6a and b, respectively. For symmetry reasons, only half of the Debye ring is shown in the plots. Results are presented in terms of the lattice parameter of the cubic cell, $a = d_{hkl}\sqrt{h^2 + k^2 + l^2}$, to allow comparison between the two plane families. The plots are similar for both rings: a large oscillation of the lattice parameter is observed for the hydrides precipitated in the original plate [1](Z3, red circles), which falls in amplitude for the hydrides precipitated in the HAZ of the weld (Z2, blue triangles). The results for the hydrides near the fusion line (Z1, black open circles) are more erratic, and error bars have been omitted for the sake of clarity. The Z1 points are dispersed around the value $a_{Z1} = 4.7577$ Å without a definite trend. Table 1 compiles the information presented in Fig. 6. The table lists the azimuthally averaged lattice parameter a for the three samples, calculated from the two reflections. Also included in the table are the values measured along the ND and RD, a_{ND} and a_{RD}, estimated as the average of ±20° around those directions. The average lattice parameter of the hydride clearly increases from the parent material (Z3) towards the fusion line (Z1). The same trend is observed for the value of a_{ND}, while exactly the opposite behaviour is observed for a_{RD}. The difference between the ND and RD directions, i.e., the amplitude of the oscillations observed in the plots, is also listed in the table as a strain amplitude $\Delta a = 2(a_{ND} - a_{RD})/(a_{ND} + a_{RD})$, with $1\ \mu\varepsilon = 10^{-6}$. The large strain amplitude present in the hydrides in the parent plate (Z3 ~4500 με) is drastically reduced in the hydrides

[1] For interpretation of color in Fig. 6, the reader is referred to the web version of this article.

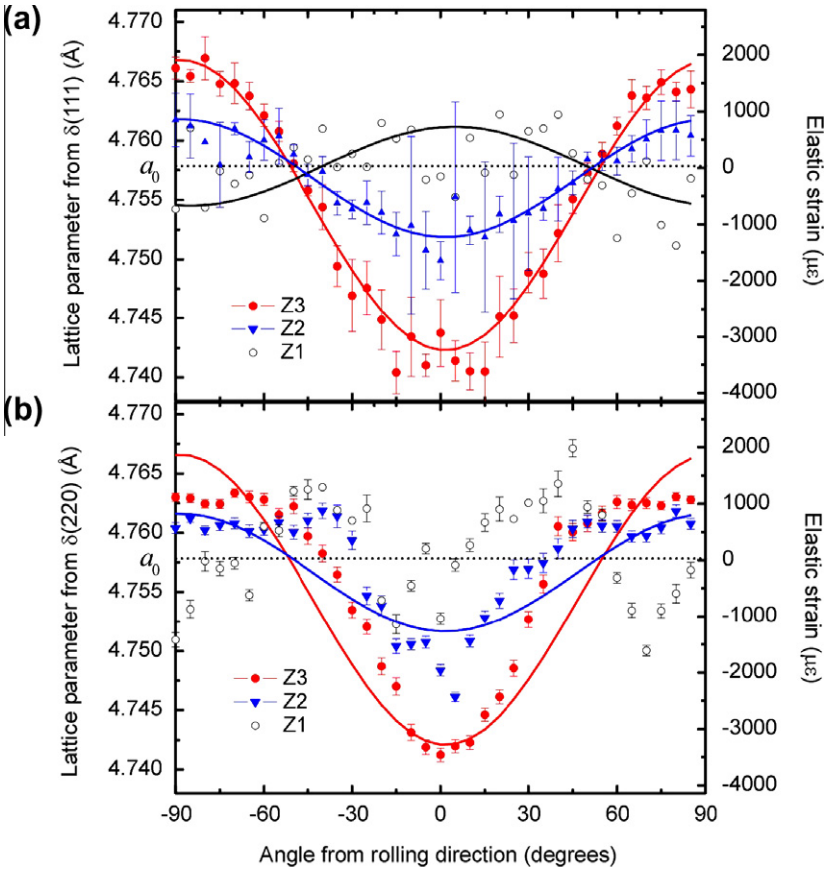

Fig. 6. Variation in the lattice parameter around Debye rings for the three specimens, indicating the presence of residual stresses for the hydrides precipitated in the Z3 and Z2 specimens. Values are derived from: (a) the δ(1 1 1) ring and (b) the δ(2 2 0) ring.

precipitated near the FZ (Z1 ~ -600 με). There are also slight but systematic differences between the lattice parameter calculated from the two hydride reflections, with a maximum difference of ~ 900 με for the Z3 specimen. These results suggest that the hydrides in the original plate are subjected to inter-granular compressive stresses along the RD, which relax across the HAZ of the weld. Hence, the oscillations observed in the plots for the Z3 and Z2 specimens are ascribed to an elastic strain field existing within the hydrides on the ND–RD plane of the plates. It was assumed that the hydrides in the Z1 specimen are nearly stress free, and the value of a_{Z1} defined above was adopted as the unstressed lattice parameter for the hydride. A justification for such an assumption is given in the next section. Using this value, the elastic strain $\varepsilon(\phi) = (a(\phi) - a_{Z1})/a_{Z1}$ can be directly read from the right axis of Fig. 6. The solid lines plotted in Fig. 6a are least-squares fits to the experimental data using the equation describing the angular dependence of a biaxial strain field, $\varepsilon(\phi) = \varepsilon_{RD}\cos^2\phi + \varepsilon_{ND}\sin^2\phi + \tau\sin 2\phi$, which provides the strain values ε_{RD} and ε_{ND} along the ND and RD, respectively, and a shear component τ. For the δ(1 1 1) ring, the curves describe the results of the Z3 and Z2 specimens very well. A very small shear component τ in both cases confirms that the RD and ND are the principal strain axes. The model is not very good for the Z1 specimen owing to the rapid variation in the experimental data. For the Z3 specimen, the fit gives $\varepsilon_{RD} = (-3200 \pm 100)$ με and $\varepsilon_{ND} = (1900 \pm 100)$ με, but one must keep in mind that these values depend on the choice for the unstressed lattice parameter a_0. The strain amplitude $\Delta\varepsilon = (\varepsilon_{ND} - \varepsilon_{RD}) = (5100 \pm 200)$ με, independent of the a_0 value, can be used for an estimation of the magnitude of the stresses, $\sigma = E{\cdot}\Delta\varepsilon/(1+\nu)$. The elastic constants of the hydride are quite close to those of the Zr matrix, i.e., $E = 97$ GPa for Young's modulus and $\nu = 0.3$ for Poisson's ratio [7]. From those values, it is estimated that the hydrides precipitated in the original plate are subjected to compressive stresses of (-360 ± 20) MPa along the RD of the plate. These grain stresses are supposed to be exerted by the α-Zr grains as a constraint to the growth of the hydride phase along the RD of the plate, as discussed in the next section.

However, the angular dependence observed for the δ(2 2 0) ring presents a rather triangular shape which is not properly captured by the biaxial strain equation referred to above. This is in line with micromechanical modelling theories of cubic crystallites, which clearly show that {1 1 1} diffraction planes are much less sensitive than {2 2 0} planes to the elastic and plastic heterogeneities resulting from texture. This means that the hydrides contributing to the δ(2 2 0) ring are not experiencing a unique elastic strain field, as could be expected from the pole figure results, which showed that the δ(2 2 0) pole figure is domi-

nated by a texture component along ND which cannot be directly derived from the α-Zr ODF. In Fig. 5, that "preferential" texture component also manifested as a δ(1 1 1) pole along the RD, which would be responsible for the slight flattening of the Z3 strain curve ~0° in Fig. 6a.

Table 1 also lists the peak full width at half maximum (FWHM) of the δ(1 1 1) and δ(2 2 0) hydride peaks measured along the RD and ND. The width is expressed in terms of the dimensionless quantity ($\Delta r/r$), with r and Δr the position (i.e., radius of the ring) and width of the peak, respectively. The widths are corrected by the instrument resolution, estimated by subtracting the FWHM measured on Ceria powder for the same Bragg angle (3000 με for the δ(2 2 0) reflection). The hydride widths are an order of magnitude larger than those of the Zr matrix, i.e., 550 με for the α(1 0 −1 0) peak close to δ(1 1 1) peak; and 800 με for α(1 1 −2 0) close to δ(2 2 0). The δ(2 2 0) widths are almost twice the value of the δ(1 1 1) peaks. There are also well-defined differences between the two directions, but without a plausible pattern.

4.3. Dissolution/precipitation

Further insight into the origin of the hydride stresses can be gained from the results of the dissolution/precipitation cycles performed in situ. Fig. 7 summarizes the experimental results obtained for the thermal cycles performed on the Z3 specimen, i.e., the original plate. Fig. 7a shows the dependence of the volume fraction of δ hydrides on the specimen temperature. The dissolution stage is represented by red solid circles, and after a hold period of 10 min at 400 °C, is followed by a precipitation stage represented by blue open circles. The difference between the two curves reveals the hysteresis typical of precipitation–dissolution processes of zirconium hydride in zirconium [15]. Identical colours are used in all plots to differentiate between the dissolution and precipitation stages. Almost identical results were obtained for three thermal cycles performed between 100 °C and 400 °C, corroborating the reversibility of the process. The two vertical lines drawn in the figure correspond to the temperatures of terminal solid solubility during the dissolution (TSSd) and precipitation (TSSp) of the hydrides reported in Ref. [15] for 180 wt. ppm of H in zircaloy-4. No significant changes in the hydride texture were observed through the thermal cycles. Fig. 7b presents the variation in the hydride lattice parameter along the ND and RD, for the hydrides responsible for the "preferential" texture component discussed in Fig. 5. So the value of a_{ND} comes from the δ(2 2 0) ring, while a_{RD} comes from the δ(1 1 1) ring. The behaviour of the hydride lattice parameter between room temperature and 400 °C is complex, with a marked hysteresis, and cannot be described by a simple coefficient of thermal expansion. On heating, the lattice parameter steadily decreases along the ND and increases along the RD. The two values equalize at TSSp (~310 °C). For higher temperatures, a_{RD} becomes slightly larger than a_{ND}, in contrast to the room temperature results. On cooling, there is a

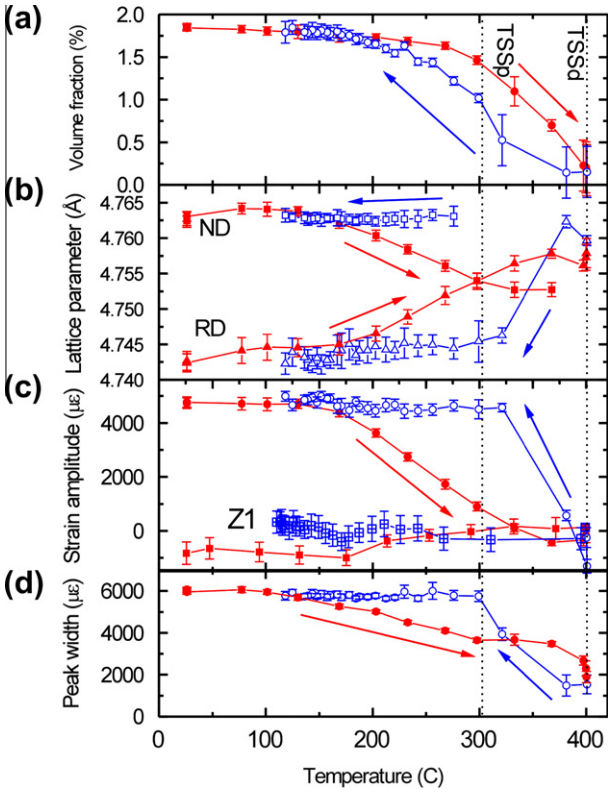

Fig. 7. Results of the dissolution (red)/precipitation (blue) tests performed in situ on the Z3 specimen. (a) Hydride volume fraction, obtained from comparison of the δ(1 1 1) and α(1 0 −1 0) peak areas. (b) Lattice parameter along RD and ND for hydrides in the texture component discussed in the text. (c) Difference in the lattice parameter along the ND and RD for the "bulk" hydrides. The results obtained for the Z1 specimen are also included for comparison. (d) Average peak width of the δ(1 1 1) Debye ring. (For interpretation of the references to colour in this figure legend, the reader is referred to the web version of this article.)

sharp change in lattice parameter at TSSp, where the hydrides essentially reach their room-temperature values along both ND and RD. The strain hysteresis is not restricted to this "preferential" texture component. Fig. 7c reveals the evolution of the strain amplitude Δε discussed in Fig. 6a, which provides the behaviour of the "bulk" hydrides. The strain amplitude Δε is equivalent to the difference between the ND and RD curves shown in Fig. 7b. Again, a clear hysteresis is observed between heating and cooling for the bulk hydrides precipitated in the original plate. The inter-granular strains gradually relax on heating, starting ~140 °C, and change sign between 340 °C and 400 °C. The abrupt change at the TSSp temperature is also repeated on cooling, where the hydrides reach the room-temperature strain amplitude. Fig. 7d shows an almost identical step for the average width of the δ(1 1 1) peaks in both position (~TSSp) and height (~4300 με). The results in Fig. 7 indicate that there are two distinct regimes during hydride precipitation: (i) a first stage between TSSd and TSSp, where stresses rapidly change with temperature; and (ii) a second stage from TSSp to completion, where stresses within the hydrides remain essentially constant. These two stages are

not observed for the hydrides precipitated in the HAZ of the weld, which has been included for comparison in Fig. 7c, with square symbols labelled as Z1. For this specimen, the strain amplitude stays relatively low and does not show hysteresis.

5. Discussion

The results presented in Fig. 7 can be explained by a simple model for hydride precipitation/dissolution based on the hydride microstructures presented in Figs. 1 and 2. In this model, after formation of a nucleus at a suitable site, there is an initial precipitation stage described by the auto-catalytic nucleation process proposed by Perovic et al. [5]. On this stage, which develops between TSSd and TSSp, thin hydride plates start growing on a plane and eventually becomes the hydride platelet revealed by optical microscopy. For the hydrides precipitated in the original plates (Z3), this plane is predominantly the RD–TD plane observed for the intra-granular hydrides seen in Fig. 2. The stress field experienced by the hydrides at this stage is complex, as it results from interaction of an expanding platelet and the surrounding Zr matrix. As shown in Fig. 2, the planar expansion of the platelets is arrested at the grain boundaries, which in doing so exert compressive stresses on the hydrides, on the RD–TD plane of the rolled plate. Subsequent growth of the hydrides would then occur by an increase in the platelet thickness, under compressive stresses that are essentially dictated by the grain size of the host material. So from TSSp to room temperature, hydride growth takes place through a relatively homogeneous precipitation of new hydrides onto the existing platelets. The appearance of a compressive biaxial stress field on the RD–TD plane after the platelet is arrested can explain the steps observed both in strain amplitude (Fig. 7c) and in peak width (Fig. 7d). Moreover, as there is no equivalent to the auto-catalytic mechanism during hydride dissolution, the hydrides dissolve isotropically upon heating. So the stresses exerted by the surrounding Zr grains on the hydride decrease in proportion to the hydride volume fraction, producing a steady decrease in strain amplitude and peak width on heating. The model also explains the high repeatability observed for the three thermal cycles, because the α-Zr grain size remains constant for the temperatures involved in these experiments. This simple model can also explain the results observed for the hydrides grown on the HAZ of the weld (Z1 curves, in Fig. 7c). As shown in Fig. 1b, owing to the large grain size found in this specimen, the grain boundaries do not constrain the growth of the hydride platelets, so no stresses are measured for the hydrides precipitating in this specimen.

The hysteresis observed in the hydride peak width gives an insight into the origin of the large peak broadening observed for the hydride phase. The value of 6000 με for the δ(1 1 1) peak width measured at the start of the thermal cycle (Fig. 7d) must be compared with the value of 550 με measured for the α(1 0 −1 0) Zr peak in the same material and for almost the same diffraction angle. Several reasons could contribute to peak broadening: (i) hydride size; (ii) arrangement and density of dislocations, i.e., type III stresses; (iii) grain stresses along directions not contained within the diffraction plane; or (iv) stress gradients within the hydrides. The δ(1 1 1) peak width decreases to reach a value of 1900 με at ~400 °C during dissolution, while on precipitation it quickly returns to the 6000 με value at ~300 °C. The similarity in the behaviour of strain amplitude and peak width suggests that the large hysteresis in peak width is related to grain stress, though it is not possible to decide whether the broadening is due to the reasons (iii) or (iv) above. Provided the Zr grains are rather circular in the RD–TD plane of the plate [12], one expects grain boundaries to impose roughly the same stress for any direction on this plane. So the large change in peak width is likely to be due to the presence of stresses along directions not contained within the diffraction plane. Regarding the remaining 1900 με of the δ(1 1 1) peak, a proper identification of its origin is not possible with the present experimental results. However, one can estimate the different contributions from information reported in the literature. TEM observations of δ hydrides in zircaloy 2 containing ~60 wt. ppm of H showed hydride platelet thickness between 2000 Å and 3000 Å [22], which could account for such a peak broadening. But the large difference in width between the δ(1 1 1) and δ(2 2 0) peaks reported in Table 1 is most likely due to different contrast factors of edge type dislocations, as the {1 1 1} planes and [1 1 0] directions conform to the most common slip system in fcc crystals.

Regarding the texture analysis presented in Fig. 5, one must recall the excellent agreement observed for the Z1 specimen between the experimental hydride pole figures and the pole figures derived from the α-Zr ODF, via the δ(1 1 1)//α(0 0 0 1) and δ[0 1 1]//α[1 1 −2 0] orientation relationship. It is worth noting that mostly intra-granular hydrides were observed in the Z1 specimen (Fig. 1b), while both inter- and intra-granular hydrides are present in the Z3 specimen (Fig. 2). So a possible interpretation of the texture results is that the pole figures derived from the α-Zr ODF represent the intra-granular hydrides, which indeed are proportional to the bulk Zr and hence to the α-Zr pole figures. By contrast, the extra texture component observed for the Z3 specimen not accounted for by the calculation would correspond to inter-granular hydrides, as they were clearly visible for this specimen.

Finally, it has been suggested that these low-concentration hydrides that grow as small precipitates within the Zr matrix should be under compression, since hydride precipitation represents a net volume expansion relative to the zirconium replaced. This suggestion casts some doubts on the choice of unstressed lattice parameter, as large hydrostatic compressive stresses could exist within the hydrides which would not be manifest in the present experiment. However, companion experiments performed on hydride blisters grown on Zr–2.5%Nb pressure tubes support our choice [23]. No compressive stresses are expected for bulk hydrides, as there is not enough α-Zr to constrain the

hydride phase. The experiments on the blister showed little difference between the average lattice parameter measured for bulk hydrides (those inside the blister) and low-concentration hydrides (those far from the blister). A difference of 800 με in the value of a measured for bulk and low-concentration hydrides has to be compared with a strain difference of ~17,000 με measured for the lattice parameter along the two principal axes on the low-concentration hydrides reported in Ref. [23]. These observations indicate that the stresses exerted by the Zr matrix on the hydride precipitates are indeed compressive but relatively directional, and limit the importance of a purely hydrostatic compressive component.

6. Conclusions

The crystallographic texture and the stresses experienced by hydrides precipitated in zircaloy-4 containing ~200 wt. ppm of hydrogen were studied. The study was based on a thorough analysis of synchrotron X-ray diffraction experiments performed with monochromatic X-ray beam and a fast area detector. The hydride texture was obtained from an analysis of the systematic intensity variations around Debye rings, while the hydride stress state was derived from the small distortion of the rings. The results showed that hydrides precipitated on rolled zircaloy-4 plates are under compressive biaxial stresses of (360 ± 20) MPa on the RD–TD plane of the plates. The origin of these stresses was examined by following the variation in the elastic strain field during the dissolution and precipitation of the hydrides for thermal cycles performed in situ between room temperature and 400 °C. The hydride stresses displayed large hysteresis, with a steady decrease in the elastic strains on heating, and an abrupt change observed on cooling, at the temperature of TSSp. The effect of the zircaloy-4 microstructure on the hydride stresses was studied by performing experiments on small coupons presenting different α-Zr grain sizes, obtained from two locations of the HAZ weld. Almost zero stresses were found for the hydrides precipitated in the HAZ close to the weld line. The experiments suggested that hydrides stresses decrease in inverse form to the grain size of the Zr matrix, so stresses were explained by the constraint imposed by grain boundaries on the growth of hydride platelets on the RD–TD plane of the plates. The magnitude of the hydride stresses is then essentially dictated by the grain size of the α-Zr matrix. Based on these ideas, the dissolution/precipitation results were explained by an initial nucleation stage occurring mainly on the RD–TD plane of the α-Zr grains, followed by an increase in thickness perpendicular to that plane. The initial growth stage is consistent with an auto-catalytic nucleation process previously proposed in the literature.

Acknowledgements

The authors whish to thank A. Motta, K. Colas, M.R. Daymond and M. Kerr for experimental help and fruitful discussions. This research was funded by a Panamerican Collaboration Program funded by CONICET, Argentina under Res 1161/07, with corresponding funding from NSERC and National Science Foundation for the Canadian and American partners. Usage of the Advanced Photon Source was supported by the US Department of Energy, under Contract No. DE-AC02-06CH11357.

References

[1] Ells CE. J. Nucl Mater 1968;28:129.
[2] Hardie D, Shanahan MW. J Nucl Mater 1975;55:1.
[3] Chu HC, Wu SK, Kuo RC. J Nucl Mater 2008;373:319.
[4] Westlake DG. J Nucl Mater 1968;26:208.
[5] Perovic V, Weatherly GC, Simpson CJ. Acta Metall 1983;31:1381.
[6] Steuwer A, Santisteban J, Preuss M, Peel M, Buslaps T, Harada M. Acta Mater 2009;57:145.
[7] Kerr M, Daymond MR, Holt RA, Almer J. J Nucl Mater 2008;380:70.
[8] Kerr M, Daymond MR, Holt RA, Almer J, Stafford S, Colas KB. Scr Mater 2009;61:939.
[9] Kerr M, Daymond MR, Holt RA, Almer J, Stafford S. Scr Mater 2010;62:341.
[10] Steuwer A, Daniels JE, Peel MJ. Scr Mater 2009;61:431.
[11] Kaufmann PD, Danielson P, Baroch EF, ASTM, ASTM STP 551; 1974. p. 52.
[12] O. Zanellato. Ph D Thesis. United Kingdom: The Open University; 2009.
[13] Woo OT, Tangri K. J Nucl Mater 1979;79:83.
[14] Haeffner DR, Almer JD, Lienert U. Mater Sci Eng A 2005;399:120.
[15] Vizcaíno P, Banchik AD, Abriata JP. Metall Mater Trans A 2004;35:2343.
[16] Daum RS, Chu YS, Motta AT. J Nucl Mater 2009;392:453.
[17] Ischia G, Wenk HR, Lutterotti L, Berberich F. J Appl Crystall 2005;38:377.
[18] Hielscher R, Schaeben H. J Appl Crystall 2008;41:1024.
[19] Vicente-Alvarez MA. Acta Metall, submitted for publication.
[20] Une K, Nogita K, Ishimoto S, Ogata K. J Nucl Sci Technol 2004;41:731.
[21] Coleman C, Doubt G, Fong R, Root J, Bowden J, Sagat S et al. In: 10th Int Symp Zirconium Nuclear Industry, ASTM STP 1245; 2004. p. 264.
[22] Perovic V, Weatherly GC. J Nucl Mater 1984;126:160.
[23] Santisteban JR, Steuwer A, Domizzi G, Peel M. Pow Diffract J 2009:24.